# Global Systematics of Copper in Arc Magmas: A Big Data Approach

Nicholas D. Barber[1*], Marie Edmonds[1], Frances Jenner[2], Andreas Audétat[3], and Helen Williams[1]

[1]Department of Earth Sciences, University of Cambridge

[2]School of Environment, Earth, and Ecosystem Sciences, The Open University

[3]Bayerisches Geoinstitut, University of Bayreuth

September 16th, 2020

## Abstract

Copper, sourced from porphyry deposits formed in arc settings, is an increasingly scarce yet critical resource. The processes that shape the copper contents of magmas remain poorly understood. One theory is that magmas must be copper-rich in order to form porphyry deposits. Mature arcs have up to now played an outsized role in shaping existing models of copper systematics in magmas. Here we take a Big Data approach, compiling multiple data sets of volcanic whole rock compositions using open-source software. We show the global ubiquity of the "copper paradox," where rocks with high Sr/Y (and high ore potential) have the lowest copper concentrations. These calc-alkaline, ore-forming magmas undergo iron depletion caused by extensive amphibole and/or garnet fractionation, promoting sulphide fractionation and copper depletion. Despite their paucity in copper, these magmas are associated with porphyry deposits, implying that magma fertility depends on factors other than a magma's bulk copper content.

## Proposed Petrological Controls on Cu in Arc Systems

Copper (Cu) is economically important owing to its role in the development of electrical components and its critical status in the transition to green energy[1]. Porphyry deposits, which are temporally and spatially associated with arc magmatism (Figure 1), account for over 70% of global Cu ore production[2], and significant amounts of Au and Mo[2]. Consensus on the mechanisms that underlie the link between arc magmatism and porphyry deposits is lacking[3]. Prevailing models of Cu porphyry formation focus on two important processes, which may promote Cu enrichment and transport into exploitable porphyry stocks, respectively: (i) the saturation of the magma in sulphide, into which Cu partitions strongly (discussed in more detail in the Supplement), which principally removes Cu from magmas, but may also at as a pre-concentration mechanism[4–7]; and (ii) the formation of an exsolved, saline hydrous or aqueous vapor phase, into which Cu and other metals partition and eventually lead to ore deposition[8–11].

What is essential in each of these processes is the petrological mechanisms which drives a system towards or away from "ore fertility;" or the capacity of a magma to be able to form a Cu ore deposit. For example, it has recently been suggested that sulfide saturation may be avoided by simultaneous Fe depletion and auto-oxidation by garnet fractionation[12]. Garnet's preference for $Fe^{2+}$ leaves residual magmas enriched in $Fe^{3+}$; this in turn produces a more oxidized, evolved melt (with higher $S^{6+}/S^{2-}$), which pushes the magma further away from sulphide saturation and may even trigger the dissolution of existing sulphides, thereby enriching the melt in Cu which could be transferred to fluids when porphyry formation commences[12]. Critically, this model like others assumes that a magma with lower Cu concentrations due to sulphide crystallization will be less likely to achieve ore fertility. However, other studies have de-emphasized the importance of magmatic metal contents as controls on later

fertility[13,14], promoting instead the importance of magmatic water content[15–17], time scales of magma differentiation[18], and larger magma volumes[19]. Nonetheless, nearly all models agree that the process of sulphide saturation is critical for understanding eventual ore formation. Sulphide saturation is a complex process mediated by temperature, pressure, and silicate melt composition, but which is increasingly well characterized[20–22]. However, it is presently unclear (i) what petrological processes in arc magmas will promote sulphide fractionation, and (ii) whether the fractionation of a sulphide, and associated loss of Cu, is detrimental to later porphyry formation.

These problems are matched by a measure of sample bias in our existing understanding of Cu systematics. Crucially, we need to establish what generic petrological processes, if any, can explain the abundances of Cu in ore fertile magmas in all major subduction zones. This understanding is needed to assess whether magmatic Cu contents themselves are a driver of or a signal for magmatic ore fertility. In order to address this need, we present a Big Data compilation of arc magma features. Our final ArcMetals database (N = 55,795) contains data from 17 arcs, encompassing geochemical and contextual information such as major, trace element and radiogenic isotope compositions, geology, location, and geologic age(see Methods). Combined, these parameters allow us to explore Cu systematics in all arc settings. We use this dataset to analyze the systematics of Cu with respect to arc magma differentiation processes. This work highlights the power of Big Data in uncovering important trends in existing petrological datasets, and provides a framework for further interrogation of chalcophile behaviour in specific volcanic arcs.

## Defining Ore Potential

It has been shown that Cu-fertile magmas (magmas that are capable of forming porphyry-Cu deposits) have high whole rock Sr/Y ratios at intermediate to felsic magma compositions (Figure 2,[16,23]). The Sr/Y ratio, which compares the Large Ion Lithophile Element (LILE) Sr to the high field strength element (HFSE) Y, is widely regarded as a proxy for high pressure fractionation of hydrous arc magmas[7,16,23]. Strontium abundances during fractionation are controlled by plagioclase[24], whereas Y abundances are controlled primarily by amphibole and garnet, as well as some minor phases like titanite[25]. The ratio of plagioclase to amphibole crystallized in a fractionating arc magma is depressed under conditions of high $H_2O$ activities[26], which breaks the polymerized chains needed to stabilize plagioclase feldspar[27], and simultaneously stabilizes amphibole phases which incorporate $H_2O$ into their structure[28]. Thus, a hydrous magma should see abundant amphibole fractionation early in its differentiation in the mid to deep crust (up to 50 km.,[29]) and late-stage plagioclase crystallization at or near volatile saturation in the upper crust[16]. This fractionation sequence will result in an elevated Sr/Y ratio, where Y is depleted due to partitioning into amphibole and Sr is enriched due to the lack of plagioclase fractionation[16].

A 'high ore potential field' has been defined in terms of whole rock Sr/Y and $SiO_2$ content for the entire global database following the approach of previous work (Figure 2a[16] which focused primarily on the Central Andes). When the global database is compared to these criteria, we see that in general, high Sr/Y magmas show an association with continental arcs such as Mexico, the Andes and the Cascades (Figure 2b and Supplementary Material), a low mean whole rock Cu concentration ($< 50$ ppm) (Figure 2c), and thicker crust (mean 40 km, Figure 2d). The mean Cu and mean crustal thickness of the high and low ore fertility groups in Figures 2c and 2d have been compared, respectively, using an

analysis of variance test (ANOVA, see Methods for details), and have all been shown to be statistically significant ($p \ll 0.005$) (Supplementary Information). The low mean Cu concentrations ([Cu]) in whole rocks associated with higher Sr/Y (Figure 2c) highlights the so-called 'Cu-paradox'[12] where Cu is present in low abundance in the magmas that appear to be most capable of forming ore deposits. An important feature of our analysis is that none of samples included come from ore deposits - thus, this Cu loss cannot be attributed simply to Cu loss to an ore forming fluid. Observations such as these have been used to support porphyry formation models where crystallization of sulphide removes Cu from the silicate melts, to be later remobilized by one of several petrological processes[4–6,12]. However, it is also possible that melt [Cu] depletion may have little bearing on whether a magma goes on to form an ore deposit[13,14]. While it is clear magmatic [Cu] is significantly lower in high Sr/Y magmas on a global scale, the petrological processes driving this association remain poorly understood. Below, we apply our large dataset to udnerstand what other signals are associated with high Sr/Y and ore fertility.

## Differentiation and Fe-Loss

Globally, both low Cu (Figure 3a) and high Sr/Y (Figure 3b) signatures can be observed to follow a calc-alkaline path, showing consistent Fe loss with decreasing [MgO] (paralleling the high Sr/Y ellipse in Figure 3d). In Figure 3c and 3d we plot the binned FeO and MgO concentrations that have been smoothed to show average FeO, MgO, Cu (Figure 3c), and crustal thickness (Figure 3d) at 0.05 wt.% MgO intervals. Figure 3c also shows that the fractional crystallization paths of experimentally synthesized and oxidized andesites and basalts[30], which also lie on the calc-alkaline trend displayed by high potential (high Sr/Y) magmas. Along the calc-alkaline differentiation path, Fe depletion appears inti-

mately tied with a depletion in Cu. Notably, our new data compilation can be used to demonstrate that the high Sr/Y magmas are following the Fe-depleting calc-alkaline differentiation trend. This finding is supported by recent work, focused on ore mineralization, which has found that calc-akaline magmas are 4 to 10 times more likely to form a viable porphyry copper deposit as tholeiitic magmas[17]. Our observation provides us with a global profile of high ore potential magmas - they are experiencing simultaneous Cu and Fe-loss as they evolve.

## Petrological Controls - Garnet and Amphibole

We can identify the mineral phases responsible for the geochemical trends shown in Figure 3 using rare earth element (REE) concentrations. The schemes at the top of both Figures 4 and 5 show vectors for the fractionation of garnet, amphibole, olivine, plagioclase, orthopyroxene and clinopyroxene using an index of REE plot curvature called Dy/Dy*[31]. Essentially, Dy/Dy* estimates the relative depletion of the middle rare earth (MREE) Dy in relation to its light and heavy counterparts (see the Methods section for details). Additionally, we plot the trajectories for melting in the garnet source field following[31]. The ratio Dy/Dy* tends to be lowered by amphibole and clinopyroxene fractionation. These same phases will deplete Dy relative to Yb. Olivine, plagioclase, and orthopyroxene will drive Dy/Dy* towards higher values, as these phases do not incorporate Dy into their structure and thus Dy will be enhanced relative to light (LREE) and heavy (HREE) rare earth elements. Garnet fractionation will move Dy/Yb to higher values during fractionation (i.e. deplete Yb relative to Dy) while simultaneously increasing Dy/Dy*. Mantle melting in the presence of garnet will lead to more moderate values if a garnet rich source is extensively melted.

The field of high Sr/Y whole rocks is shown by the ellipse in Figure 4b. Our global dataset suggests that high Sr/Y arc magmas share key petrological features: they may be produced from garnet-rich mantle source regions (plotting in the lower right quadrant of figure 4); undergo extensive fractionation of amphibole +/- garnet (they extend into the bottom left quadrant for Figure 4, upper right in Figure 5); and in keeping with their high ore potential profile, develop low Cu abundances (Figure 4a, 5a). While there is a clear association between high Sr/Y, low Cu magmas and the amphibole fractionation field, the location of ore fertile magmas at low Dy/Dy* and moderate Dy/Yb can also be explained through a magma formed in the "melting of mantle garnet" field (bottom right quadrant) which subsequently experienced (1) garnet fractionation at pressures $> 1.2$ GPa[32], followed by (2) amphibole fractionation at lower pressures[32]. This sequence may only be piecemeal at shallower pressures, where amphibole will predominate as a fractionating phase, because garnet will not be stable[32]. Thus, while we will shortly demonstrate the importance of amphibole in these systems, garnet likely also plays an important role, especially under higher pressures[12,33].

The REE systematics of the global database can be further explored using a statistical approach[34], which compares parameters describing the shape of chrondrite-normalized multi-REE plots. A schematic at the top of Figure 5 shows the effect of fractionation of amphibole and garnet on REE systematics, expressed in terms of $\lambda 1$ and $\lambda 2$. Figure 5 is subsampled to only color magmas for Cu (Figure 5a) and Sr/Y (Figure 5b) where the whole rock composition shows ore-fertile Sr/Y signatures (Sr/Y $> 50$). Interestingly, whole rocks with the highest Sr/Y ratios are characterized by concave-up REE profiles, where there is both HREE depletion and overall enrichment in the REE . Figure 4 shows a strong preference for high Sr/Y magmas to sit in the bottom right

quadrant (High Dy/Yb, low Dy/Dy*), and Figure 5a and 5b show many high Sr/Y whole rocks sitting near the amphibole fractionation and garnet source field in $\lambda 1$ vs. $\lambda 2$ space (higher $\lambda 1$, higher $\lambda 2$). It is important to keep in mind that clinopyroxene will drive many of these REE trends in the same direction, whether in Dy/Dy* or $\lambda$ space. However, clinopyroxene is less stable at lower temperatures[30,32], and amphibole is increasingly stabilized with greater water concentrations[30,32].

Garnet fractionation has gained popularity in the recent literature as a potential ore fertility mechanism[12,33,35]. Experiments have shown that garnet is stabilized as a fractionating phase at pressures above 1.2 GPa (approximately 42 km. depth)[32,36] and where melt water contents are high (above 4 wt. %)[32]. Direct evidence of garnet in arc magmas is rarely found in modern volcanic systems, but it has been found commonly in fossil arc systems[37]. Whether ancient or modern, where garnet can be seen widely in arc systems is in the lower crust cumulate lithologies of exhumed "arc roots," sections like the type section in Kohistan, Pakistan[38]. Models developed for the mantle wedge underlying Central America found evidence for the presence of mantle heterogeneities rich in garnet-peridotite or garnet pyroxenite lithologies[39]. Such mantle garnet "veins" would impart a garnet fingerprint on the resultant magmatic REE abundances if tapped by melting[39]. Despite these suggestions for the importance of garnet fractionation and mantle garnet melting, we suggest that amphibole is more likely candidate for moderating global arc REE systematics as shown in Figures 4 and 5. Amphibole is common and fractionates in any arc magmatic environment at moderate depths, while also being verifiable petrographically in volcanic products. These trends do not preclude the importance of garnet or clinopyroxene fractionation, but clearly show the strong and unambiguous importance of the association between amphibole and high ore fertility magmas.

To validate this framework, it is necessary to show how amphibole can provide a mechanistic link between the different features for a high ore fertility magma's profile, as we have see from Figures 2 through 5.

## The Importance of Sulphur

Sulphide saturation in a melt is described by the experimental parameter, "sulphur content at sulphide saturation," or SCSS[40]. The SCSS is negatively correlated with pressure[40] and positively correlated with temperature[21,40,41], melt $H_2O$ content[42], melt FeO, Cu and Ni contents[21,40,43]20,21,43, and oxygen fugacity ($fO_2$)[22,41]. For mid-ocean ridge basalts, melt FeO content, oxygen fugacity ($fO_2$), temperature, and pressure are the main drivers of sulphide saturation[43]. In arc magmas, higher water and sulfur contents[8,44] coupled with higher oxidation state[13,22] cause the SCSS to respond differently as compared to MORB. For most arc magmas, volatile and oxidation conditions lie outside the range for which many SCSS models are calibrated[40], with some exceptions[22,42]. Since most arc magmas have a considerable fraction of sulphur present as $S^{6+}$, they may instead saturate in anhydrite, which is much more soluble in silicate melts[45].

Like garnet, amphibole is much more stable at high $H_2O$[30,32,36], but unlike garnet it predominates at moderate depths (20-55 km.[29,32]). We have modeled the trace element abundances of experimental results from an existing study to constrain the effect of amphibole on the liquid line of descent in arc magmas, in order to understand how amphibole fractionation may connect major and trace element systematics under high ore potential conditions[30]. The experimental study in question ran isobaric experiments under equilibrium (EC) and fractional crystallization (FC) conditions at 1.0 GPa on hydrous basaltic[46] and andesitic melts[47]30. Given the mineral proportions and glass compositions reported from[30], we modeled the effect of phases like amphibole on SCSS, major,

and trace element abundances as they appear on the liquidus (Figure 6, symbolized curves in Figure 3, orange field in Figure 5). These modeled effects of amphibole can be compared to generic differentiation trends in major elements and [Cu] (Figure 3) to determine what specific process is driving [Cu] depletion across all subduction zones. In order to develop these curves, we applied a simple fractional crystallization model following[48] for the trace elements Cu, Ni, Sr, Y, and all REEs (model details in Supporting Information).

We used the major element glass compositions produced at each step of the experiments to model SCSS using the equations of[20], which relates SCSS as a function of FeO, MgO, Cu, Ni, and temperature (Methods). For all experiments, SCSS decreases with FeO and decreasing temperature (Figure 6a and 6b respectively)[40]. These SCSS values are initially calculated assuming the redox state of the magma will favor mainly $S^{2-}$[20]. To correct for this in the more oxidized experimental runs[30], we used an $S^{6+}$ correction[49] (see Methods for details) to determine realistic SCSS curves for more oxidized arc magmas, at $S^{6+}$ proportions of 10, 50, and 90% of total sulphur (green curves with different symbols in Figure 6a, 6b). We mark the onset of amphibole crystallization in each run and its effect on whole rock FeO concentration using grey boxes. High-temperature (>1050 °C) FeO loss is attributed to clinopyroxene, followed by a much more dramatic lowering of SCSS at amphibole-in. These two FeO loss trends are separated by an abrupt decrease in SCSS, which is a function of temperature change as clinopyroxene abundance decreases and amphibole starts to appear (blue curve in Figure 6a). The onset of amphibole fractionation is associated with a dramatic lowering of the SCSS (Figure 6a). We prefer amphibole over clinopyroxene as the mineral phase linking Figures 4-6, as clinopyroxene in these models only fractionates at temperatures greater than 1050 °C. Since arc magmas usually contain bulk sulphur contents of > 1000 ppm (red line

in Figures 6a and 6b)[44], these models confirm that most hydrous arc magmas are at or near sulphide saturation[13] during differentiation, and as a result will become depleted in Cu as sulphides are removed. The presence of sulphides in magmas has been reported by an increasing number of studies, in areas as diverse as Western North America[35], Kīlauea[49], the Ecuadorian Andes[50], and even sulphide-rich hornblende cumulates porphyry deposits[14,51].

Even accounting for the uncertainty in the oxidation state of the magmas that produced the whole rocks in the global database, there is compelling evidence that amphibole fractionation drives cal-alkaline differentiation, extensive sulphide fractionation, and subsequent melt [Cu] depletion. It is worth noting that this model of amphibole mediating SCSS and, by extension other chalcophiles, follows similar approaches[6]. Another Fe-rich mineral, magnetite, has been implicated in taking up substantial quantities of $Fe^{3+}$, which has been shown to lead to reduction of S from $S^{6+}$ to $S^{2-}$. Since sulphide saturates at much lower [S] as compared to sulphate[6], like our oxidized andesite models, higher proportions of $S^{2-}$ will promote sulphide fractionation and metal loss. The crucial difference is that amphibole's ability to promote sulphide fractionation and Cu loss is due to its reduction of total melt [FeO], as opposed to models involving the fractionation of high $Fe_3^+/Fe_{tot}$ phases like magnetite.

## Global Cu Control

Our Big Dataset demonstrates that high Sr/Y magmas experience abundant amphibole fractionation, which may in turn promote sulphide fractionation. The sulphide we focus on in this case is crystalline sulphide (e.g. monosulphide solid solution; MSS) which should predominate the the lower temperature conditions of an arc magmas as compared to MORB[51–54]. Is there direct evidence linking MSS fractionation with Cu depletion in arc magmatic sequences? In Figure 7, we

plot whole rock Cu/Ag vs. MgO , coloured for both Gd/Yb (Figure 7a), Dy/Dy* (Figure 7b), and for crustal thickness (CT) (Figure 7c). The motivation behind constructing such plots stem from the fact that Cu fractionates more strongly into MSS than Ag[55], and such a ratio gives us the benefit of sensitively detecting the presence of a fractionating MSS at sulphide saturation. A low Cu/Ag ratio, below average mid-ocean ridge basalt (MORB)[56,57] and continental crust[58], is consistent with crystalline sulphide fractionation and consequent Cu removal from the silicate melt[57]. Gd/Yb (Figure 7a) is a proxy for garnet involvement in petrogenesis because Gd partitions less strongly into garnet than Yb[56], and has been used to infer the prevalence of garnet fractionation in the Andes[33].

The highest Gd/Yb ratios are associated with whole rocks with the lowest Cu/Ag for a given MgO content (Figure 7a), suggesting a direct correlation between the proportion of garnet fractionation and the proportion of sulfide fractionation. Owing to the complexities in analysing whole rocks for Ag, Cu/Ag datasets are rare and are currently biased towards the Andes data, though there are some measurements in other transitional arcs (Figure 7 symbols). There is no clear link between Cu/Ag in the whole rock and crustal thickness, but the very thickest crust (>40 km) is associated with evolved volcanic rocks with in general a high Gd/Yb (indicating garnet in the source or garnet fractionation) and low Cu/Ag. Figure 7b shows that lower Dy/Dy*, indicative of amphibole, is also associated with low Cu/Ag, evolved magmas. Thus, both garnet and amphibole are implicated in the petrogenesis of magmas that have experienced the most sulphide fractionation.

Our schematic model outlining the primary importance of amphibole fractionation, and the secondary importance of garnet fractionation and garnet in the mantle source is shown in Figure 8. We emphasize the importance of amphibole as a universal petrological mechanism that explains all the features of our

high ore potential profile. The global applicability of our amphibole-centred model addresses some of the concerns surrounding garnet alone being a vector for Cu depletion[12]. A fundamental point arising from this analysis is the observation that whole-rock Cu concentrations are negatively correlated with inferred porphyry Cu fertility. Some previous studies[12] have implicitly assumed that early sulphide saturation is detrimental to eventual porphyry copper deposit development, articulating the 'Cu paradox,' of low magmatic [Cu] being associated with ore deposits[12]. Studies using platinum group elements as proxies for sulphide saturation in arc systems make this assumption explicit, arguing that ore development requires late sulphide saturation[5]. However, as suggested in recent work[14], porphyry systems that have experienced both prolonged amphibole fractionation and early sulphide crystallization (and subsequent Cu loss) seem perfectly capable of developing porphyry deposits later in their lifetime[14]. Our global database demonstrates that melt Cu concentration does not act as a primary control on porphyry fertility, in agreement with the observation that high ore fertility magmas not only have lower Cu concentrations (Figure 3c), but that combined amphibole/garnet fractionation can lead directly to early sulphide saturation. The low magmatic Cu concentrations we observe in the ore-fertile magmas in our database are thus reflective of processes like amphibole fractionation that are associated with ore formation.

## Conclusion

In this study we present a comprehensive geochemical and geophysical database of volcanic whole rock samples across 17 arcs covering most of the Earth's active subduction zones. This database, ArcMetals, allows for flexible investigation of co-variations in tectonics, storage conditions, chemistry, and spatial distribution of around 55,000 samples covering the compositional ranges from basalt to rhy-

olite. Here we presented the first order features of this global dataset to identify the key petrological processes that control [Cu] in arc magmas, which may help to guide future investigations. High ore potential magmas show geochemical evidence for having been generated in hydrous, possibly garnet-bearing, mantle wedges. More importantly, there is a strong association between high ore potential, calc-alkaline differentiation, and amphibole +/- garnet fractionation. High ore potential magmas show depletion of Fe during calc-alkaline differentiation and are associated with significantly lower whole rock mean Cu concentrations and thicker continental crust. These trends are driven by extensive amphibole fractionation, which lowers melt Fe contents and hence SCSS, driving sulphide saturation and Cu removal into sulphides. In conjunction with this, the hydrous composition of the source region could promote the stabilization of garnet in the mantle source, while high water contents in a high pressure magma could promote both amphibole and garnet fractionation. Garnet fractionation can also contribute to Fe depletion, and subsequently increases the likelihood of sulphide saturation at greater depths before amphibole fractionates. However, garnet fractionation is restricted to high pressures and may not occur in all arcs[12]. This question of prevalence emphasizes that amphibole is a better vector for explaining global Cu systematics, as any arc magma with enough water will fractionate amphibole at intermediate compositions. Importantly, the global dataset indicates that amphibole fractionation is, irrespective of the presence of garnet on the liquidus, capable of lowering SCSS and promoting early sulphide saturation. Magmatic Cu contents are thus reflective of the crucial petrological processes identified in our global database and are not a driver or proxy for ore fertility.

Our analysis of the ArcMetals dataset also demonstrates that while many arc magmas fractionate amphibole and most (if not all) arc magmas are rich

in water and other volatiles, porphyry deposits remain rare. Furthermore, our study demonstrates early sulphide saturation is not necessarily detrimental to later porphyry formation from a typical calc-alkaline arc magmas. Even more crucial is the tectonic (e.g. compressional stresses), geodynamic, geological, and temporal conditions of the magma reservoir system itself[14,16,59], which along with the geochemical factors analyzed here, strongly influence whether or not a porphyry system will form. It is possible that porphyry mineralization requires long timescales for differentiation and fluid segregation[16,59] under conducive crustal configurations, which could promote further amphibole crystallization in a melt-rich mid-crustal hot zone[59]. Larger magma volumes may be optimal for achieving extreme volatile concentration[60] (e.g. minimum 1000 $km^3$ for Bingham Canyon and other large porphyry deposits[18,59]), which would also favor porphyry mineralization[14,16,17,59]. Such high water contents could promote extreme amphibole fractionation and subsequent sulphide fractionation, and would be reflected in the high Sr/Y signal from porphyry fertile magmas.

# References


1. Arndt, N. T. *et al.* Future global mineral resources. *Geochemical Perspectives* **6,** 1–171 (2017).

2. Singer, D. A., Berger, V. I., Menzie, W. D. & Berger, B. R. Porphyry copper deposit density. *Economic Geology* **100,** 491–514 (2005).

3. Hedenquist, J. W. & Lowenstern, J. B. The role of magmas in the formation of hydrothermal ore deposits. *Nature* **370,** 519–527. ISSN: 0028-0836. http://www.nature.com/doifinder/10.1038/370519a0 (Aug. 1994).

4. Wilkinson, J. J. Triggers for the formation of porphyry ore deposits in magmatic arcs. *Nature Geoscience* **6,** 917. http://dx.doi.org/10.1038/

ngeo1940%20http://10.0.4.14/ngeo1940%20https://www.nature.com/articles/ngeo1940#supplementary-information (Oct. 2013).

5. Park, J.-W. *et al.* Chalcophile element fertility and the formation of porphyry Cu±Au deposits. *Mineralium Deposita* **54,** 657–670 (2019).

6. Jenner, F. E., ONeill, H. S. C., Arculus, R. J. & Mavrogenes, J. A. The magnetite crisis in the evolution of arc-related magmas and the initial concentration of Au, Ag and Cu. *Journal of Petrology.* ISSN: 00223530 (2010).

7. Chiaradia, M. Copper enrichment in arc magmas controlled by overriding plate thickness. *Nature Geoscience* **7,** 43–46 (2014).

8. Edmonds, M. & Mather, T. A. Volcanic sulfides and outgassing. *Elements.* ISSN: 18115217 (2017).

9. Blundy, J., Mavrogenes, J., Tattitch, B., Sparks, S. & Gilmer, A. Generation of porphyry copper deposits by gas–brine reaction in volcanic arcs. *Nature Geoscience* **8,** 235–240 (2015).

10. Nadeau, O., Williams-Jones, A. E. & Stix, J. Sulphide magma as a source of metals in arc-related magmatic hydrothermal ore fluids. *Nature Geoscience.* ISSN: 17520894 (2010).

11. Audetat, A., Pettke, T., Heinrich, C. A. & Bodnar, R. J. Special paper: the composition of magmatic-hydrothermal fluids in barren and mineralized intrusions. *Economic Geology* **103,** 877–908 (2008).

12. Lee, C.-T. A. & Tang, M. How to make porphyry copper deposits. *Earth and Planetary Science Letters* **529,** 115868 (2020).

13. Richards, J. P. The oxidation state, and sulfur and Cu contents of arc magmas: implications for metallogeny. *Lithos* **233,** 27–45 (2015).

14. Du, J. & Audétat, A. Early sulfide saturation is not detrimental to porphyry Cu-Au formation. *Geology* **48,** 519–524 (2020).

15. Richards, J. P. Magmatic to hydrothermal metal fluxes in convergent and collided margins. *Ore Geology Reviews* **40,** 1–26 (2011).

16. Loucks, R. Distinctive composition of copper-ore-forming arcmagmas. *Australian Journal of Earth Sciences* **61,** 5–16 (2014).

17. Rezeau, H. & Jagoutz, O. The importance of H2O in arc magmas for the formation of porphyry Cu deposits. *Ore Geology Reviews,* 103744 (2020).

18. Chelle-Michou, C., Rottier, B., Caricchi, L. & Simpson, G. Tempo of magma degassing and the genesis of porphyry copper deposits. *Scientific reports* **7,** 40566 (2017).

19. Steinberger, I., Hinks, D., Driesner, T. & Heinrich, C. A. Source plutons driving porphyry copper ore formation: combining geomagnetic data, thermal constraints, and chemical mass balance to quantify the magma chamber beneath the Bingham Canyon deposit. *Economic Geology* **108,** 605–624 (2013).

20. O'Neill, H. The thermodynamic controls on sulfide saturation in silicate melts with application to Ocean Floor Basalts. (2020).

21. Smythe, D. J., Wood, B. J. & Kiseeva, E. S. The S content of silicate melts at sulfide saturation: new experiments and a model incorporating the effects of sulfide composition. *American Mineralogist* **102,** 795–803 (2017).

22. Jugo, P. J., Wilke, M. & Botcharnikov, R. E. Sulfur K-edge XANES analysis of natural and synthetic basaltic glasses: Implications for S speciation and S content as function of oxygen fugacity. *Geochimica et Cosmochimica Acta* **74,** 5926–5938 (2010).

23. Richards, J. P. High Sr/Y ratio magmas and porphyry Cu, Mo, Au Deposits:Just add water. *Economic Geology* **106,** 1075–1081. ISSN: 0361-0128. http://dx.doi.org/10.2113/econgeo.106.7.1075 (Nov. 2011).

24. Ewart, A. & Griffin, W. Application of proton-microprobe data to trace-element partitioning in volcanic rocks. *Chemical Geology* **117,** 251–284 (1994).

25. Green, T. H. Experimental studies of trace-element partitioning applicable to igneous petrogenesis—Sedona 16 years later. *Chemical Geology* **117,** 1–36 (1994).

26. Grove, T., Parman, S., Bowring, S., Price, R. & Baker, M. The role of an H 2 O-rich fluid component in the generation of primitive basaltic andesites and andesites from the Mt. Shasta region, N California. *Contributions to Mineralogy and Petrology* **142,** 375–396 (2002).

27. Stolper, E. Water in silicate glasses: an infrared spectroscopic study. *Contributions to Mineralogy and Petrology* **81,** 1–17 (1982).

28. Foden, J. & Green, D. Possible role of amphibole in the origin of andesite: some experimental and natural evidence. *Contributions to Mineralogy and Petrology* **109,** 479–493 (1992).

29. Santana, L. V., McLeod, C., Blakemore, D., Shaulis, B. & Hill, T. Bolivian hornblendite cumulates: Insights into the depths of Central Andean arc magmatic systems. *Lithos,* 105618 (2020).

30. Ulmer, P., Kaegi, R. & Müntener, O. Experimentally derived intermediate to silica-rich arc magmas by fractional and equilibrium crystallization at 1· 0 GPa: An evaluation of phase relationships, compositions, liquid lines of descent and oxygen fugacity. *Journal of Petrology* **59,** 11–58 (2018).

469 31. Davidson, J., Turner, S. & Plank, T. Dy/Dy*: variations arising from man-
470 tle sources and petrogenetic processes. *Journal of Petrology* **54,** 525–537
471 (2013).

472 32. Alonso-Perez, R., Müntener, O. & Ulmer, P. Igneous garnet and amphibole
473 fractionation in the roots of island arcs: experimental constraints on an-
474 desitic liquids. *Contributions to Mineralogy and Petrology* **157,** 541 (2009).

475 33. Cox, D. *et al.* Elevated magma fluxes deliver high-Cu magmas to the upper
476 crust. *Geology* **48** (2020).

477 34. O'Neill, H. S. C. The smoothness and shapes of chondrite-normalized rare
478 earth element patterns in basalts. *Journal of Petrology* **57,** 1463–1508
479 (2016).

480 35. Chen, K. *et al.* Sulfide-bearing cumulates in deep continental arcs: The
481 missing copper reservoir. *Earth and Planetary Science Letters,* 115971
482 (2019).

483 36. Greene, A. R., DeBARI, S. M., Kelemen, P. B., Blusztajn, J. & Clift, P. D.
484 A detailed geochemical study of island arc crust: the Talkeetna arc section,
485 south–central Alaska. *Journal of Petrology* **47,** 1051–1093 (2006).

486 37. Bissig, T., Leal-Meja, H., Stevens, R. B. & Hart, C. J. High Sr/Y magma
487 petrogenesis and the link to porphyry mineralization as revealed by Garnet-
488 Bearing I-type granodiorite porphyries of the Middle Cauca Au-Cu Belt,
489 Colombia. *Economic Geology* **112,** 551–568 (2017).

490 38. Ducea, M. N., Saleeby, J. B. & Bergantz, G. The architecture, chemistry,
491 and evolution of continental magmatic arcs. *Annual Review of Earth and*
492 *Planetary Sciences* **43,** 299–331 (2015).

493 39. Feigenson, M. D. & Carr, M. J. The source of Central American lavas:
494 inferences from geochemical inverse modeling. *Contributions to Mineralogy*
495 *and Petrology* **113,** 226–235 (1993).

496 40. O'Neill, H. & Mavrogenes, J. A. The sulfide capacity and the sulfur content
497 at sulfide saturation of silicate melts at 1400 C and 1 bar. *Journal of*
498 *Petrology* **43,** 1049–1087 (2002).

499 41. Nash, W. M., Smythe, D. J. & Wood, B. J. Compositional and tempera-
500 ture effects on sulfur speciation and solubility in silicate melts. *Earth and*
501 *Planetary Science Letters* **507,** 187–198. ISSN: 0012-821X. http://www.
502 sciencedirect.com/science/article/pii/S0012821X18307155 (2019).

503 42. Fortin, M.-A., Riddle, J., Desjardins-Langlais, Y. & Baker, D. R. The effect
504 of water on the sulfur concentration at sulfide saturation (SCSS) in natural
505 melts. *Geochimica et Cosmochimica Acta* **160,** 100–116 (2015).

506 43. Kiseeva, E. S., Fonseca, R. O. & Smythe, D. J. Chalcophile elements and
507 sulfides in the upper mantle. *Elements* **13,** 111–116 (2017).

508 44. Wallace, P. J. & Edmonds, M. The sulfur budget in magmas: evidence from
509 melt inclusions, submarine glasses, and volcanic gas emissions. *Reviews in*
510 *Mineralogy and Geochemistry* **73,** 215–246 (2011).

511 45. Zajacz, Z. & Tsay, A. An accurate model to predict sulfur concentration at
512 anhydrite saturation in silicate melts. *Geochimica et Cosmochimica Acta*
513 **261,** 288–304 (2019).

514 46. Hürlimann, N. *et al.* Primary magmas in continental arcs and their differ-
515 entiated products: petrology of a post-plutonic dyke suite in the Tertiary
516 Adamello batholith (Alps). *Journal of Petrology* **57,** 495–534 (2016).

517 47. Baker, M. B., Grove, T. L. & Price, R. Primitive basalts and andesites from
518 the Mt. Shasta region, N. California: products of varying melt fraction and

water content. *Contributions to Mineralogy and Petrology* **118,** 111–129 (1994).

48. Shaw, D. M. *et al. Trace elements in magmas: a theoretical treatment* (Cambridge University Press, 2006).

49. Wieser, P., Jenner, F., Edmonds, M., Maclennan, J. & Kunz, B. Chalcophile elements track the fate of sulfur at Kilauea Volcano, Hawai'i (2020).

50. Georgatou, A., Chiaradia, M., Rezeau, H. & Wälle, M. Magmatic sulphides in Quaternary Ecuadorian arc magmas. *Lithos* **296,** 580–599 (2018).

51. Chang, J. & Audétat, A. Petrogenesis and metal content of hornblende-rich xenoliths from two Laramide-age magma systems in southwestern USA: insights into the metal budget of arc magmas. *Journal of Petrology* **59,** 1869–1898 (2018).

52. Keith, M., Haase, K. M., Klemd, R., Schwarz-Schampera, U. & Franke, H. Systematic variations in magmatic sulphide chemistry from mid-ocean ridges, back-arc basins and island arcs. *Chemical Geology.* ISSN: 00092541 (2017).

53. Rottier, B., Audétat, A., Koděra, P. & Lexa, J. Origin and Evolution of Magmas in the Porphyry Au-mineralized Javorie Volcano (Central Slovakia): Evidence from Thermobarometry, Melt Inclusions and Sulfide Inclusions. *Journal of Petrology* **60,** 2449–2482 (2019).

54. Li, Y. & Audétat, A. Gold solubility and partitioning between sulfide liquid, monosulfide solid solution and hydrous mantle melts: Implications for the formation of Au-rich magmas and crust–mantle differentiation. *Geochimica et Cosmochimica Acta* **118,** 247–262 (2013).

55. Patten, C., Barnes, S.-J., Mathez, E. A. & Jenner, F. E. Partition coefficients of chalcophile elements between sulfide and silicate melts and

the early crystallization history of sulfide liquid: LA-ICP-MS analysis of MORB sulfide droplets. *Chemical Geology* **358,** 170–188 (2013).

56. Jenner, F. E. *et al.* Chalcophile element systematics in volcanic glasses from the northwestern Lau Basin. *Geochemistry, Geophysics, Geosystems.* ISSN: 15252027 (2012).

57. Jenner, F. E. Cumulate causes for the low contents of sulfide-loving elements in the continental crust. *Nature Geoscience.* ISSN: 17520908 (2017).

58. Holland, H. D. & Turekian, K. K. Treatise on geochemistry (2004).

59. Chiaradia, M. & Caricchi, L. Stochastic modelling of deep magmatic controls on porphyry copper deposit endowment. *Scientific reports* **7,** 1–11 (2017).

60. Rohrlach, B. D., Loucks, R. R. & Porter, T. Multi-million-year cyclic ramp-up of volatiles in a lower crustal magma reservoir trapped below the Tampakan copper-gold deposit by Mio-Pliocene crustal compression in the southern Philippines. *Super porphyry copper and gold deposits: A global perspective* **2,** 369–407 (2005).

# Methods

## Data Sources and Compilation

### Geochemistry

Sample geochemical and analytical data were collected from the GeoRoc ([1]) database. These data were compiled using open source python code, available on GitHub (see link). Initially, 19 arc magma datasets were included in the database, but the Kermadec and Banda files contained so few data upon filtering, that they were ultimately omitted. Data for both arc volcanic and plutonic

rocks as well as for xenoliths were compiled (see Supporting Info). Before filtering, the fully compiled database contained > 200,000 records. In order to maximize the number of measurements per sample, we applied six filters to the initial compilation: (1) records with data obtained before 1960 C.E. were removed; (2) records with no recorded analytical technique were removed; (3) only those records pertaining to measurements by X-ray fluorescence (XRF), secondary ion mass spectrometry (SIMS), electron microprobe (EPMA), thermal ionization mass spectrometry (TIMS), inductively-coupled plasma mass spectrometry (ICP MS), laser ablation inductively-coupled plasma mass spectrometry (LA ICP MS), and Fourier transform infra red (FTIR) spectroscopy were retained; (4) the database was reduced to individual records where sample name, material type (whole rock, glass, or inclusion), and analytical technique were the same (e.g. if 1 whole rock sample had 4 records in GeoRoc measured using XRF, this filter would reduce the 4 records to one average for XRF); (5) records with the same sample name and material type were averaged and collapsed into one record. This had the effect of combining a sample's ICPMS measured trace elements with its XRF derived major elements; (6) samples that had the same element measured more than once using the same technique were removed. This filter only affected a small subset (a few hundred) samples, but having it in place makes it easier to quantify analytical errors (see SI). See the Supplemental Information section for more details. Before plotting the final database was filtered to only include those magma's with a reported loss on ignition (LOI) less than 3.5 wt.%, following standards in the literature[2]

## Geophysical Parameters

Several global geophysical datasets were appended to the main database using the geospatial software Quantum Geographic Information System, or QGIS 3.4[3]. The data appended included subducting slab surfaces & geometry gener-

ated from extensive seismic records (slab dip, depth to slab, slab thickness)[4] , crustal thickness ([5]), and subducting plate sediment cover thickness ([6]). Every sample record in the database was linked to the geophysical datasets, which have good global coverage at a resolution of 10-100 $km^2$. A sub-population of database records had additional geophysical data appended based on their proximity to volcanoes analyzed in Syracuse et al. 2006[7]. These data included convergence rate, slab thermal parameter, and slab age[7]. The full QGIS methods and compilation scripts can be found in the Supplementary Information Section.

## Statistics

The mean Cu concentrations in Figure 5, 6, and 7, discussed in the Supplement, as well as the other mean high vs. low ore fertility metrics in Figure 3, were compared using a two-way analysis of variance (ANOVA) hypothesis test, and subsequent Tukey's highly significant difference test. The null hypothesis tested in all cases was that the mean of a given measure is the same between two groups. The likelihood this is due to random chance is calculated using an F statistic, given by:

$$F = \frac{\Sigma n_j \left(\bar{X}_j - \bar{X}\right)^2 /(k-1)}{\sum \Sigma \left(X - \bar{X}_j\right)^2 /(N-k)}$$

,

Where $n_j$ = the sample size in the $j^{th}$ group, $\bar{X}_j$ is the sample mean in the $j^{th}$ group, $\bar{X}$ is the overall mean, k is the number of independent groups in the analysis, and N is the total number of observations in the analysis[8].

This F-statistic is compared to a a critical-F at a given confidence threshold and degrees of freedom. After determining the p-value, which is a simple but easily misinterpreted measure of the likelihood a difference between the means

occurring due to random chance, the difference between the different treatments (e.g. different arcs) is compared using a Tukey HSD test, which calculates the following test statistic:

$$q_s = \frac{Y_A - Y_B}{SE}$$

,

where $Y_A$ is the larger of the two means, $Y_B$ the smaller, and SE the standard error of the sum of the means.

See the Supporting Information for detailed plots comparing the test statistics, tables with statistical outputs and constraints, and the code used in these analyses.

## Geochemical Indices to Track Differentiation

These indices include trace element ratios (e.g. Sr/Y, Ta/Yb, Ba/Nb, etc.) calculated directly from existing data, and graphical measures (e.g. Dy/Dy*, Eu anomaly, $\lambda 0$, etc.) that require mathematical solutions.

Dy/Dy* is a geochemical index described by[9] and widely used in studies of arc magmas. The measure makes a weighted determination of the slope and shape of an REE spider plot with respect to Dy, as:

$$\frac{Dy}{Dy*} = \frac{Dy_N}{La_N^{4/13} + Yb_N^{9/13}}$$

.

Dy/Dy* is of particular use for tracking amphibole and garnet fractionation, and garnet present in the mantle source region[9–12] (See Figure 6).

The REE polynomials, symbolized by $\lambda$, describe the shape of REE curves[13] based on multivariate statistics across all REE elements[13] The polynomials are

determined from the following calculation in orthogonal form:

$$\ln([\text{REE}]/[\text{REE}]_{\text{CI}}) = \lambda_0 + \lambda_1 \text{f}_1^{\text{orth}} + \lambda_2 \text{f}_2^{\text{orth}} + \dots$$

Where the $f$ variables represent polynomials of REE atomic radius ($r_{REE}$), chosen to avoid co-correlation of the $\lambda$s[13].

## Experimental Models

Figures 8, 9, and 6 include data from Ulmer et al. 2018[14]. These data were prepared by manually transcribing Tables 1 (start conditions), Table 2 (model abundances of minerals at each experimental temperature step), and Table 3 (glass and amph compositions, determined by EPMA) into Supplemental Data Table X. In Ulmer et al. 2018, major elements were the only measured chemical species. Starting abundances of Ni, Cu, Sr, Y, and all REEs were taken from the trace element compositions of the relevant starting materials[15–17], and used to model the partitioning of trace elements into fractionating mineral phases following the methods of Shaw 2006[18] (see below) The resulting trace element abundances across each model were treated to the same analysis as the global database for trace element ratios (e.g. Dy/Dy*) and measures of REE curve shapes (e.g. $\lambda$). We also calculated SCSS folloowing[19].

### Trace Elements

To model the trace element abundances of Cu, Ni, Sr, Y, and the REE's found in experimental products of[14], we apply the Rayleigh fractionation equation presented in[18] (Equation 3.20):

$$\frac{c_l^t}{c_o} = F^{D-1}$$

,

where:

t = timestep *t* in a given experiment, corresponding to a specific set of T, P, and $X_i$ conditions. Also called *run number* in 'ud' database.

$c_l^t$ = concentration of an element in the residual liquid

$c_o$ = initial concentration of an element in bulk liquid, before fractionation

$F^t$ = fraction of residual liquid -> $\frac{L}{L_o}$

$D^t$ = "Bulk D," or weighted sum of whole rock partition coefficients, where $X_i$ = mass fraction of mineral *i* in accumulated solid fraction, ad $D^{i-l}$ = : partition coefficient (or $K_d$) between mineral *i* and liquid *l*:

$$D^t = \sum_{i=0}^{\infty} X_i^t * D_{i-l}^t$$

Final form of equation 3.20 for this model requires us to solve for $c_l$ at each experimental step (run Number) in an experiment, of which there are three experiments total in our experimental database:

$$c_l = c_o * F^{D-1}$$

## SCSS

We modeled the SCSS for the experimentla products shown in Figure 8, using the major elements[14] and modeled trace elements (Cu, Ni) of the individual products as inputs into the new SCSS paramterization of O'Neill 2020:

$$\ln\left[\mathrm{S}^{2-}\right]_{\mathrm{SCSS}} = \Delta G^{O}_{FeO-FeS}/\mathrm{RT} + \ln C_{S^{2-}} - \ln a_{FeO}^{silmelt} + \ln a_{FeS}^{Sulf}$$

This method builds on the work of[20], and is very sensitive to the sulphide

composition, and Fe-Ni-Cu partioning into that sulphide, as well as P and T at ranges appropriate for our Stage 2 model[19].

SCSS is very sensitive to oxidation state, especially in more evolved andesite[21]. To account for this, we calculated SCSS for a range of $S_6{}^+$ speciation end members (0.2, 0.5, and 0.9 in terms of S6/Stot). These are shown schematically in Figure 4, and implications are picked apart in greater detail in the Supplement. The correction for this is taken from[22]:

$$SCSS_{Tot} = \frac{SCSS^{2-}}{\left(1 - \frac{S^{6+}}{\Sigma S}\right)}$$

This in turn is based on the Jugo (2010) parameterization of S6+ as a function of ΔQFM buffer:

$$\frac{S^{6+}}{S_T} = \frac{1}{1 + 10^{(2.1 - 2\Delta FMQ)}}$$

Ulmer (2018) gives estimated ranges for the fO2 in terms of ΔNNO oxygen buffer, as between +0.5 and 1.5 for the FC experiments. Taking the equations above, our $\frac{S^{6+}}{S_T}$ ratio should be between **0.89 and 0.07** (this is all fit through Kress and Carmichaels 1991 paramterization of Fe3/Fe2 and fO2). This is a huge range, and shows that oxidation state changes radically throughout the experiments. If we assume the midpoint of this distribution, 0.5 for the sulphate/sulphide ratio, is representative, our correction involves revising up the SCSS a factor of 2 (50%), 1.11 (10%), and 10 (90%) (see Figure 8a, 8c) to model the effect of different redox conditions on our proposed amphibole control mechanism on sulphide stability.

# References


1. Sarbas, B. & Nohl, U. The GEOROC database as part of a growing geoinformatics network. *Geoinformatics* (2008).

2. Loucks, R. Distinctive composition of copper-ore-forming arcmagmas. *Australian Journal of Earth Sciences* **61,** 5–16 (2014).

3. Team, Q. D. *et al.* QGIS geographic information system. *Open source geospatial Foundation project* (2016).

4. Hayes, G. P. *et al.* Slab2, a comprehensive subduction zone geometry model. *Science* **362,** 58–61 (2018).

5. Szwillus, W., Afonso, J. C., Ebbing, J. & Mooney, W. D. Global crustal thickness and velocity structure from geostatistical analysis of seismic data. *Journal of Geophysical Research: Solid Earth* **124,** 1626–1652 (2019).

6. Pasyanos, M. E., Masters, T. G., Laske, G. & Ma, Z. LITHO1. 0: An updated crust and lithospheric model of the Earth. *Journal of Geophysical Research: Solid Earth* **119,** 2153–2173 (2014).

7. Syracuse, E. M. & Abers, G. A. Global compilation of variations in slab depth beneath arc volcanoes and implications. *Geochemistry, Geophysics, Geosystems.* ISSN: 15252027 (2006).

8. Sullivan, L. *Hypothesis Testing - Analysis of Variance (ANOVA)* https://sphweb.bumc.bu.edu/otlt/MPH-Modules/BS/BS704_HypothesisTesting-ANOVA/BS704_HypothesisTesting-Anova_print.html.

9. Davidson, J., Turner, S. & Plank, T. Dy/Dy*: variations arising from mantle sources and petrogenetic processes. *Journal of Petrology* **54,** 525–537 (2013).

10. Lee, C.-T. A. & Tang, M. How to make porphyry copper deposits. *Earth and Planetary Science Letters* **529,** 115868 (2020).

11. Chen, K. *et al.* Sulfide-bearing cumulates in deep continental arcs: The missing copper reservoir. *Earth and Planetary Science Letters,* 115971 (2019).

12. Cox, D., Watt, S. F., Jenner, F. E., Hastie, A. R. & Hammond, S. J. Chalcophile element processing beneath a continental arc stratovolcano. *Earth and Planetary Science Letters* **522,** 1–11 (2019).

13. O'Neill, H. S. C. The smoothness and shapes of chondrite-normalized rare earth element patterns in basalts. *Journal of Petrology* **57,** 1463–1508 (2016).

14. Ulmer, P., Kaegi, R. & Müntener, O. Experimentally derived intermediate to silica-rich arc magmas by fractional and equilibrium crystallization at 1· 0 GPa: An evaluation of phase relationships, compositions, liquid lines of descent and oxygen fugacity. *Journal of Petrology* **59,** 11–58 (2018).

15. Baker, M. B., Grove, T. L. & Price, R. Primitive basalts and andesites from the Mt. Shasta region, N. California: products of varying melt fraction and water content. *Contributions to Mineralogy and Petrology* **118,** 111–129 (1994).

16. Hürlimann, N. *et al.* Primary magmas in continental arcs and their differentiated products: petrology of a post-plutonic dyke suite in the Tertiary Adamello batholith (Alps). *Journal of Petrology* **57,** 495–534 (2016).

17. Grove, T., Parman, S., Bowring, S., Price, R. & Baker, M. The role of an H 2 O-rich fluid component in the generation of primitive basaltic andesites and andesites from the Mt. Shasta region, N California. *Contributions to Mineralogy and Petrology* **142,** 375–396 (2002).

18. Shaw, D. M. *et al. Trace elements in magmas: a theoretical treatment* (Cambridge University Press, 2006).

19. O'Neill, H. The thermodynamic controls on sulfide saturation in silicate melts with application to Ocean Floor Basalts. (2020).

20. Smythe, D. J., Wood, B. J. & Kiseeva, E. S. The S content of silicate melts at sulfide saturation: new experiments and a model incorporating the effects of sulfide composition. *American Mineralogist* **102,** 795–803 (2017).

21. Jugo, P. J. Sulfur content at sulfide saturation in oxidized magmas. *Geology* **37,** 415–418 (2009).

22. Wieser, P., Jenner, F., Edmonds, M., Maclennan, J. & Kunz, B. Chalcophile elements track the fate of sulfur at Kilauea Volcano, Hawai'i (2020).

23. Singer, D. A., Berger, V. I., Menzie, W. D. & Berger, B. R. Porphyry copper deposit density. *Economic Geology* **100,** 491–514 (2005).

24. Wallace, P. J. & Edmonds, M. The sulfur budget in magmas: evidence from melt inclusions, submarine glasses, and volcanic gas emissions. *Reviews in Mineralogy and Geochemistry* **73,** 215–246 (2011).

25. Jenner, F. E. Cumulate causes for the low contents of sulfide-loving elements in the continental crust. *Nature Geoscience.* ISSN: 17520908 (2017).

# Data Availability

All of our data, code, and protocols are available at the corresponding author's GitHub: https://github.com/ndb38/slab_metals. This current link is subject to change: the database and all associated code is going to be stream lined into a less crowded repository in future versions, and allowed to virtually run through Binder. The code and figures will be updated in future versions of the database, but all the material pertaining to this paper will be preserved.

## Acknowledgements

We thank Callum Reekie for providing the Python code for the SCSS models, and for useful comments on SCSS. We thank Penny Wieser for providing a critical appraisal of our early database, and helpful comments regarding the SCSS and trace elements models and their outputs. An additional thank you is extended to James Crosby and Andrew Whyte for their early comments on the importance of amphibole. We would also like to thank the attendees of Goldschmidt 2020 for their constructive and supportive comments. We acknowledge funding from the NERC Centre for the Observation and Modelling of Earthquakes, Volcanoes and Tectonics (COMET). The Gates Cambridge Trust provides financial support for NDB's PhD.


## Author Contributions

NDB conceived the project with advice and comments from ME and FJ. NDB compiled the database, wrote the Python code, and performed the analysis. ME., FJ, AA, and HW provided equal contributions regarding data interpretations and significant references. NDB wrote the manuscript with equal editing contributions from ME, FJ, AA, and HW.

## Competing Interests

The authors declare no competing interests.

## Materials and Correspondence


All correspondence should be directed to Nicholas Barber (ndb38@cam.ac.uk).

# Figures

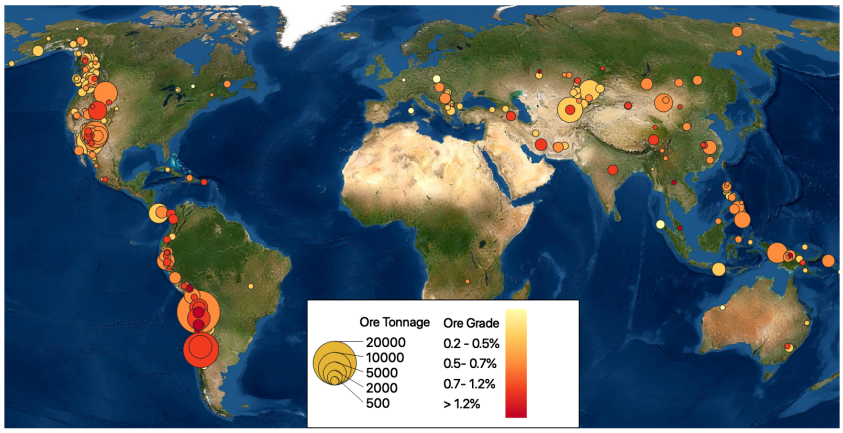


Figure 1: Map of the worlds named and prospected Cu porphyry deposits. Color of the circles corresponds to ore grade (% Cu per weight of rock removed). Size of circles corresponds to total tonnage (megatons of deposit). Data from [23]. Created using QGIS 3.4.

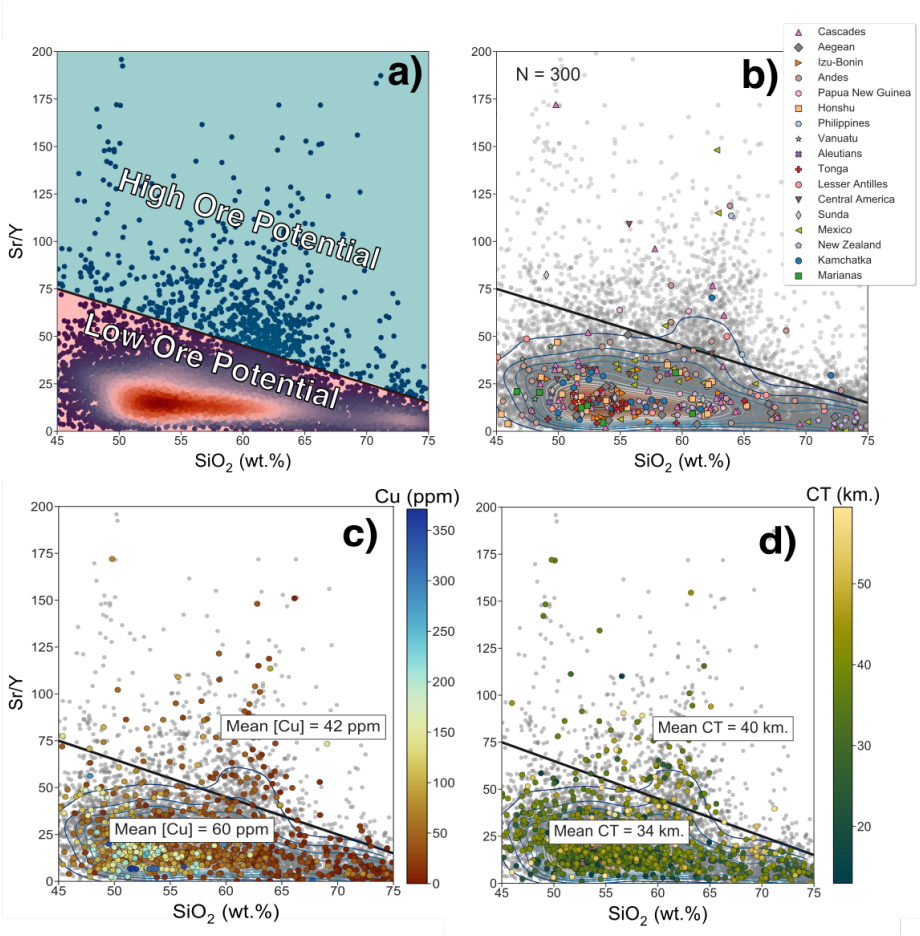


Figure 2: Sr/Y vs. $SiO_2$ plots, colored for different features. Plots b) and c) are both sub-sampled to only display 300 (b) and 1000 (c) samples for visual clarity. The black line called out in a) differentiates "high" from "low" ore potential, as defined in the literature [2]. Magmas sitting above the black line have higher ore formation potential. Plot a) is colored by the density of points in the total dataset, and contours for sample density are included in all subsequent plots. Plot b) shows a sub-sample of arc magmas colored and symbolized by arc; notice how ore-producing arcs are the only ones that tend to proliferate above the high ore potential line. Plot c) shows a sub-sample of the database colored for Cu, where high and low ore potential magmas have mean [Cu] of 42 and 60 respectively. Similarly, plot d) shows that high ore potential magmas have thicker crust, on average, than low ore potential magmas

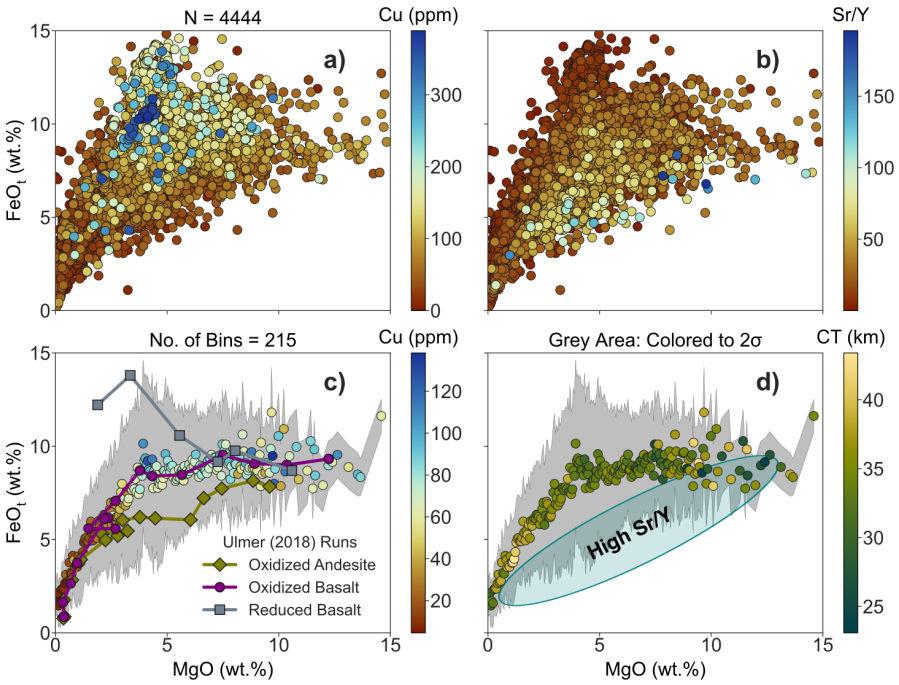


Figure 3: Differentiation trends for the entire dataset, colored for Cu in a) and Sr/Y in b). The highest Cu and Sr/Y measurements are ordered to plot on top of lower measurements. In (c) and (d), resampled averages are calculated for the full database (N = < 12,000) every 0.05 wt.% of MgO, colored for c) Cu (ppm) and d) Crust Thickness (km.). Errors colored out to $2\sigma$, smoothed by a factor of 1.5 to reduce observed spread. Superimposed on the global database (c) are the empirical results of fractional crystallization experiments in arc conditions from [14]. Like Figure 5, blue ellipse is the area where high Sr/Y magmas plot in this Figure (5d)

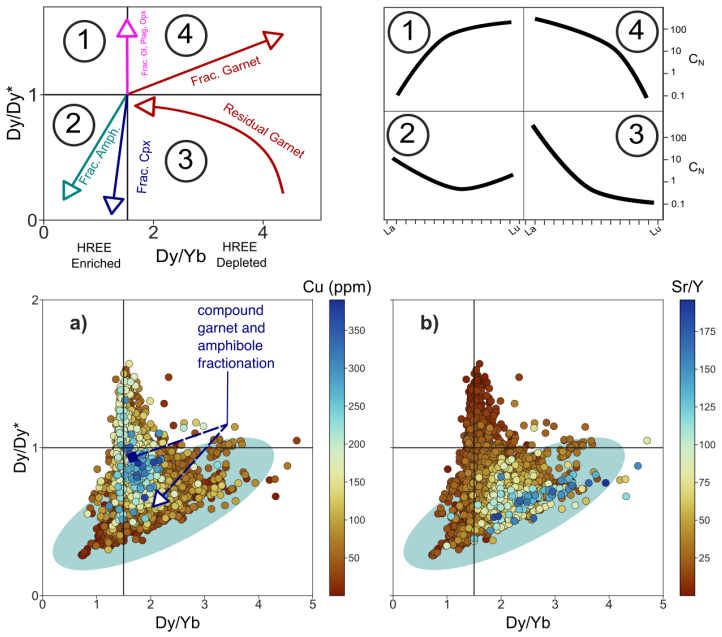


Figure 4: Panels showing the distribution of a) Cu and b) Sr/Y in Dy/Dy vs. Dy/Yb space. These Dy plots show relative fractionation trends according to which mineral phase is dominant. The starting point of each schematic mineral vector is in reference to a chrondrite normalized REE composition. The lowest Cu and highest Sr/Y magmas sit in an area generated by a combination of amphibole and garnet fractionation, and potential mantle source garnet melting. Points in a) and b) are ordered highest to lowest, with the highest Cu and Sr/Y stacked on top. Also shown as a blue ellipse is the area where high Sr/Y magmas plot in Dy/Dy* vs. Dy/Yb space. The dark blue arrow in plot a) shows the expected differentiation path of a magma ascending from high to low pressure, and experiencing first garnet, then amphibole fractionation. Such a liquid line of descent (LLD) can explain the spread in our high ore potential field.

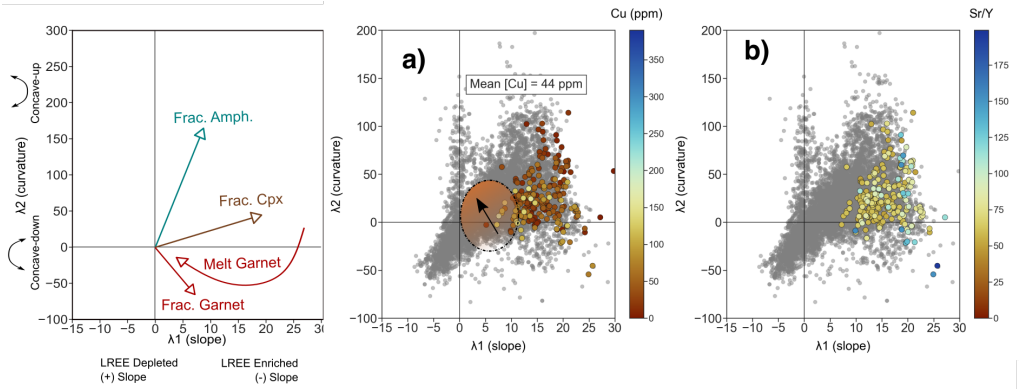


Figure 5: REE behaviour as described by $\lambda$ spider-plot shape parameters [13]. Top panels are schematics, showing how $\lambda 1$ vs. $\lambda 2$ plots describe mineralogical controls on REE's during differentiation. While $\lambda 1$ describes slope, it is calculated according to the radius of ordered REEs. Hence, a negative $\lambda 1$ corresponds to a positively sloped REE spider profile. a) and b) plot $\lambda 1$ vs. $\lambda 2$ colored for Cu and Sr/Y respectively. Grey points show the entire global database. Colored points are those that plot in the high ore potential field of Figure 3. Mean [Cu] of high Sr/Y field given in a). Empirical results from [14] are shown in the orange shaded area in Figur a) and b), where the arrow denotes the evolving REE contents of empirical products in $\lambda$ space.

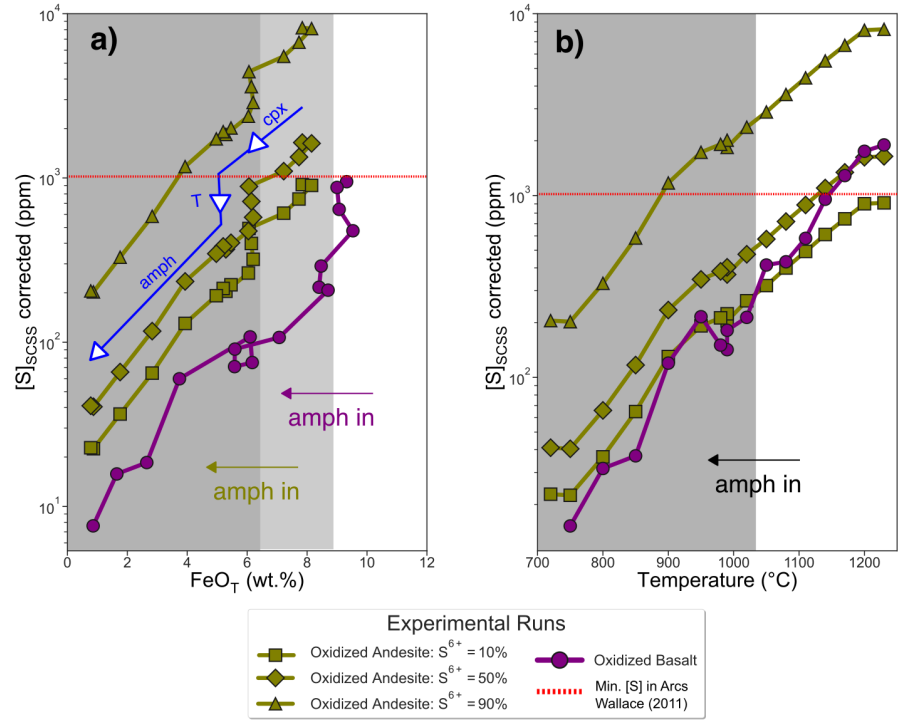


Figure 6: Empirical results of glasses from [14], using initial trace element abundances from [15–17], and the SCSS model of [19]. Plots show log(SCSS) vs. a) Total FeO and b) c) log(SCSS) vs. Temperature °C. Starting materials in each run were symbolized as: olive colored diamonds = oxidized andesite; purple circles = oxidized basalt;. Vertical grey bars indicate the onset of amphibole fractionation for the oxidized andesite vs. the oxidized basalt runs, respectively. Amphibole is measured to appear around 6.5 wt.% FeO and 1050 °C). SCSS of the model andesite was reported for 3 proportions of $S^{6+}/\Sigma S$ - 10% (squares), 50% (diamonds), and 90% (triangles) respectively, following the corrections in [22]. The red dashed line at 1000 ppm [S] is the average minimum [S] content in arc magmas, taken from [24]. Discussion of partition coefficients used to model SCSS, Cu, and Sr/Y can be found in the Methods and Supporting Information.)

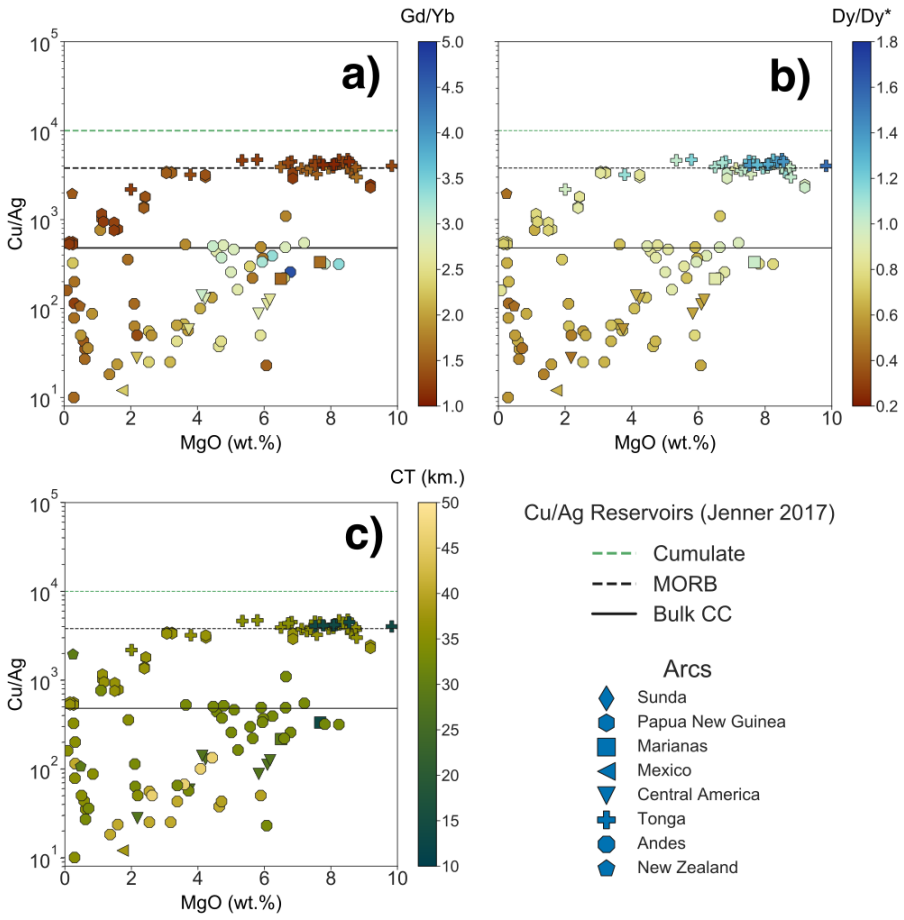


Figure 7: Cu/Ag (as a proxy for crystalline sulphide fractionation) plotted against MgO. Colored for a) Gd/Yb, b) Dy/Dy*, and c) Crust Thickness. Majority of samples plotted here are whole rock compositions. Individual samples are symbolized according to the arc they come from. Plot structure and reference lines for Cu/Ag adapted from [25], as are the reference compositions for Cu/Ag in Sulphide cumulates, MORB, and Bulk CC.

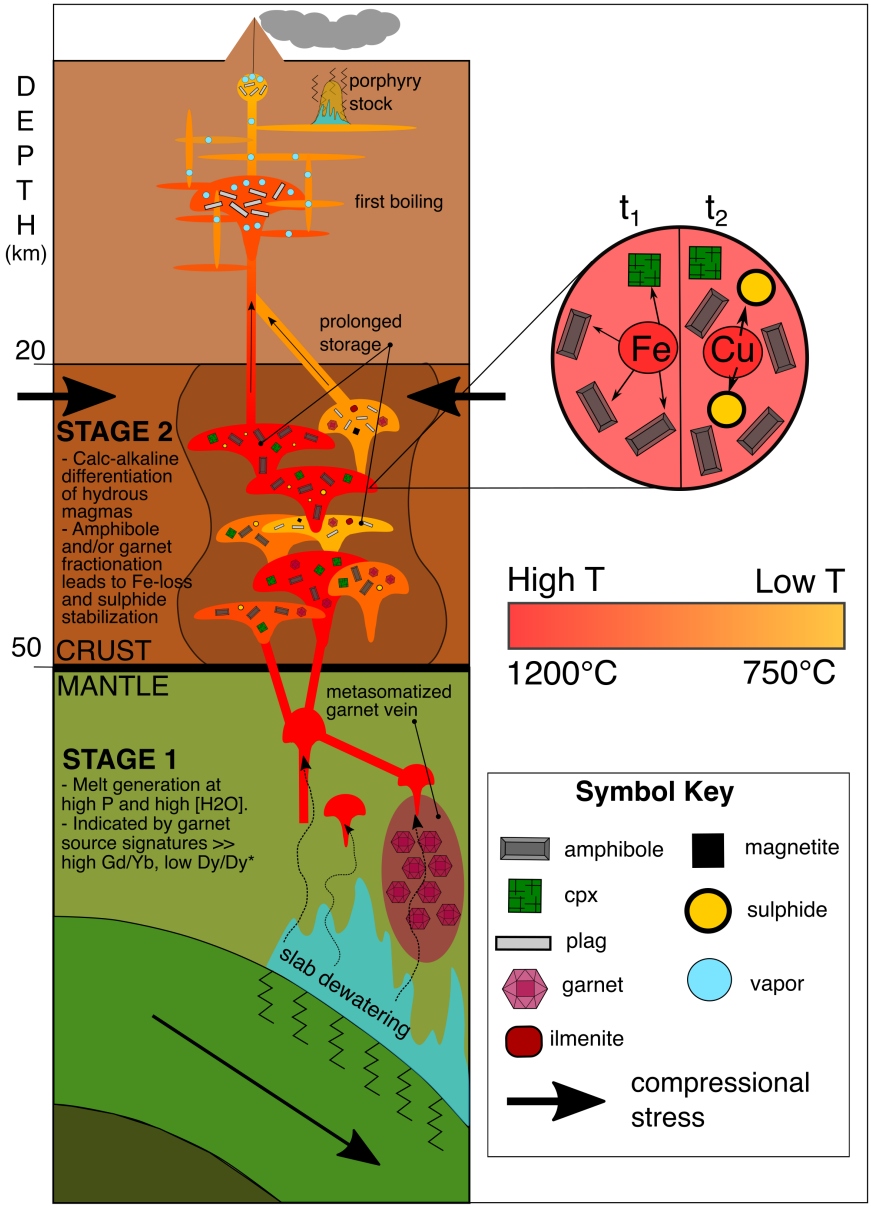


Figure 8: Our proposed model for Cu depletion in arc magmas. This model takes into account the different geochemical and geophysical signals picked out by our database. Stage 1 sees hydrous melting stabilize garnet in the mantle wedge under the right conditions, which imparts the Gd/Yb signal seen in some magmas in Figure 7. High water contents of these calc-alkaline primitive melts contribute to prolonged amphibole fractionation in Stage 2, where magmas staled at depth (=/< 1 GPa) will fractionate enough amphibole to reduce [Fe] and stabilize sulphide. garnet fractionation likely plays a role at depths > 50 km, and could similarly deplete ore-fertile magmas in Fe, leading to sulphide fractionation.